

BRISC: A Dataset of Channel Measurements at 5 GHz With a Reflective Intelligent Surface

Mattia Piana, Giovanni Angelo Alghisi, Anna Valeria Guglielmi, Giovanni Perin,
Francesco Gringoli, and Stefano Tomasin

Abstract—We introduce the broadband reconfigurable intelligent surface (RIS) channel (BRISC) dataset. The dataset comprises measurements of channel state information (CSI) collected at 5.53 GHz using a 256-element RIS with binary states. In the measurement campaign, the transmitter and receiver are two software defined radios (SDRs), phase-synchronized via an OctoClock, where the transmitter (receiver) is equipped with one (two) antenna(s). To manage complexity, the RIS elements are grouped into blocks of different sizes, where all elements within a block share the same state. CSIs have been captured for multiple a) transmitter positions (and fixed receiver location), b) pilot block sizes, and c) state configurations. Furthermore, we calibrated the parameters of state-of-the-art RIS channel models to fit the measured CSI. With approximately 10 000 configurations explored per transmitting position, BRISC serves as a robust benchmark in communication applications. We also show here an example of its use for physical-layer authentication.

Index Terms—Channel Measurements, Dataset, Physical-Layer Security, Reconfigurable Intelligent Surface.

INTRODUCTION

The evolution toward next-generation wireless systems is pushing communication networks beyond the traditional paradigm of passive propagation environments. While fifth generation (5G) systems are currently being deployed, research efforts are increasingly focusing on sixth generation (6G) technologies, where extreme flexibility, reliability, and security are expected to play a central role. In this context, reconfigurable intelligent surfaces (RISs) have emerged as a promising solution to actively shape the wireless channel by dynamically controlling the electromagnetic response of the environment. However, only a few datasets of communication channels through RISs are available, and most of them are of simulated data (e.g., [1]).

This paper introduces the broadband RIS channel (BRISC) dataset, a comprehensive collection of channel state information (CSI) measurements obtained at 5.53 GHz using a 256-element binary-state RIS. The measurement campaign uses

This work has been supported by the EU through the Horizon Europe/JU SNS project ROBUST-6G (grant no. 101139068).

Mattia Piana, Anna Valeria Guglielmi, and Stefano Tomasin are with the Dept. of Information Engineering of the University of Padova, via Gradenigo 6/b, 35131, Padova, Italy. S. Tomasin is also with the Department of Mathematics, University of Padova, Italy.

Giovanni Angelo Alghisi, and Francesco Gringoli are with the Dept. of Information Engineering of the University of Brescia, via Branze 38, 25123, Brescia, Italy.

Giovanni Perin is with the Dept. of Information Engineering of the University of Brescia, and with the Dept. of Information Engineering of the University of Padova.

phase-synchronized software defined radios (SDRs) via an OctoClock to capture data across various transmitter positions, pilot block sizes, and state configurations, where complexity is managed by grouping RIS elements into blocks of uniform states. Beyond the raw measurements, this paper validates state-of-the-art RIS channel models and algorithms to ensure alignment with empirical observations. Containing approximately 10,000 configurations per transmitting position, BRISC provides a robust benchmark for diverse communication applications, as demonstrated by a featured use case in physical layer authentication. The BRISC dataset and the script used for this analysis are available at these links [2], [3].

RIS: USAGE AND CHANNEL MEASUREMENTS

A RIS consists of a large number of sub-wavelength reflecting elements whose electromagnetic properties can be electronically tuned. By properly configuring these elements, a RIS modifies the phase—and, in practical implementations, also the amplitude—of the reflected signal [4]. This enables programmable beamforming, spatial filtering, and constructive or destructive interference [5]. Such capabilities allow the communication system to exert partial control over the propagation channel, transforming the environment from a passive medium into an active system component. RISs can also be used in indoor environments, where propagation is challenging due to the presence of reflectors, absorbers, and obstacles that generate severe multi-path fading and shadowing. In such scenarios, the channel often lacks a dominant line-of-sight (LOS) component, which typically reduces communication quality. The introduction of a RIS transforms the indoor environment from a passive obstacle to an active programmable participant in the communication process [4].

RIS-assisted communications have attracted significant attention for performance enhancement, coverage extension, and support of emerging services such as localization, sensing, and physical-layer-security (PLS). For security purposes, the RIS has been widely investigated to improve confidentiality through PLS techniques, as well as resilience against jamming and interference attacks. By controlling the propagation environment, an RIS can enhance legitimate links, suppress unintended signal leakage, and mitigate malicious interference [6]–[8]. In the following, we focus on authentication mechanisms that exploit signals passing through RIS.

As mentioned in the Introduction, the limited amount of publicly available data on CSI with RISs represents a major obstacle to reproducible research, model validation, and fair



Fig. 1. Photograph of the experimental testbed used for the measurement campaign, highlighting the transmitting antenna TX and the 16×16 RIS prototype mounted on its support structure.

comparison of signal processing, learning, and security techniques designed for RIS-assisted communications. Existing experimental works often focus on a restricted set of configurations or provide limited insight into the variability of the channel across different RIS states and transmitter (TX) locations, thus preventing exhaustive analysis and data-driven modeling. In [9], the authors employed the same RIS we used in this work, but the measurements were taken in an anechoic chamber, and only the forward transmission coefficient between the transmit and receive antenna is provided. This makes [9] a valuable dataset for the RIS radio frequency (RF) characterization, but it is rather limited for real standard-compliant indoor scenarios.

The scarcity of available datasets of channels with RIS has motivated the creation of the BRISC dataset, for which we showcase the application of tag-based physical layer authentication (PLA) in an indoor scenario, with impersonating transmitters in several positions.

EXPERIMENTAL SETUP AND DATA ACQUISITION

This section presents the experimental testbed and the measurement campaign underlying the BRISC dataset. We detail the hardware setup, the data acquisition procedure, and the strategy adopted to systematically collect raw in-phase and quadrature (IQ) recordings and CSIs under different RIS configurations and TX locations.

Fig. 1 shows a picture of the experimental setup, including the RIS, electromagnetic absorbing panels, and a horn antenna for transmission. One absorber is positioned between the TX and receiver (RX) to block the LOS between the two, thus

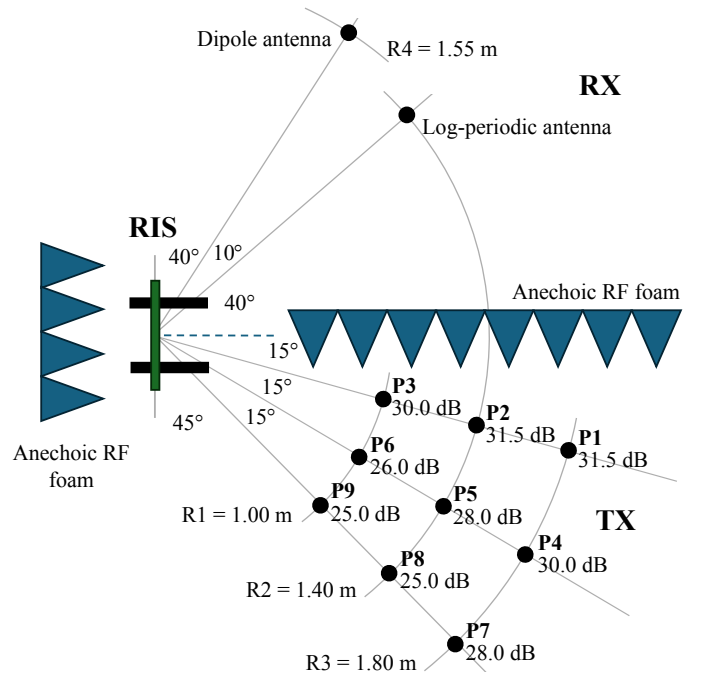


Fig. 2. Measurement setup and geometry of the experimental scenario.

allowing the RIS to have a stronger impact on the measured channel. Another absorber is positioned behind the RIS to block wall reflections and thus isolate the signal reflected by the RIS.

The experiments are conducted in a controlled indoor environment where the RIS and the RX remain fixed, while the TX is placed at nine predefined positions. A top-view of the overall setup geometry is illustrated in Fig. 2, which shows the positions of the TX, the RX, and the RIS. The multiple TX positions refer to the different locations of the single log-periodic transmitting antenna. At the RX, two antennas (a log-periodic and a dipole) are simultaneously deployed and remain fixed in position throughout the entire measurement campaign. For each TX location, a different internal SDR transmit gain was selected to adjust the signal to the dynamic range of the receiving SDR, as reported in the figure.

RIS Prototype

The RIS employed in this study is described in [10] and consists of a 16×16 array of unit cells manufactured on a low-cost flame-resistant 4 printed circuit board (PCB), for a total of 256 elements. The total surface measures 400 mm in width and 320 mm in height. A dedicated control board is mounted on the back of the panel and connected to a host computer via USB, enabling real-time reconfiguration during the measurement campaign. For mechanical stability, the surface is fixed to an acrylic support using stand-offs and nylon screws.

Each unit cell follows a three-layer PCB architecture with a plated through-hole (via) connecting the front radiating patch to the control circuitry on the backside, similar to a pin-fed patch antenna. The backside circuit integrates a complementary metal-oxide-semiconductor (CMOS)-based single-

pole double-throw (SPDT) radio-frequency switch, which toggles the element between open and short conditions, thus achieving two distinct reflection states with low power consumption.

This architecture provides 1-bit control for each element, meaning that every unit cell can be electronically switched between two discrete reflection states, resulting in different reflection coefficients that vary both in amplitude and phase. The electromagnetic response of the surface has been experimentally characterized in [10], where the complete hardware design and measurement campaign are detailed. The device has been designed to maximize the phase variation across the Wi-Fi frequency band from 5.150 GHz to 5.875 GHz.

Instrumentation Hardware and Experimental Setup

The acquisition system relies on two identical SDRs, serving as TX and RX, and specifically two Ettus USRP X310 platforms.¹

The two SDRs are synchronized using an external OctoClock,² providing a common 10 MHz reference clock and pulse-per-second (PPS) signal. This configuration ensures phase coherence between the TX and the RX, which is essential for reliable CSI acquisition and phase-sensitive measurements.

To reduce the impact of uncontrolled reflections in the indoor environment, the TX employs a highly directive log-periodic antenna (HyperLOG 60100).³ At the RX side, two different antennas are used: a directive log-periodic antenna (HyperLOG 30100)⁴ and a wideband dipole antenna. The log-periodic antenna provides spatial filtering and emphasizes the intended TX-RIS-RX path, whereas the dipole antenna, due to its broader radiation pattern, captures a richer multipath structure.

To obtain meaningful CSI measurements and accurately study the channel variations induced by the RIS, the gain of the acquisition chain must remain fixed for each transmitter position, without automatic gain control (AGC). Otherwise, variations introduced by the automatic gain control would be indistinguishable from those caused by changes in the propagation channel, preventing a reliable interpretation of the measured CSI. For this reason, the receive chain operates with AGC disabled and a fixed internal gain of 35 dB.

On the transmit side, an external linear power amplifier is used to increase the transmitted signal level. The amplifier operates in the band of 5 GHz to 5.8 GHz, with a nominal gain of 25 dB, and a maximum output power of 2 W.

Because channel attenuation varies across TX locations, the received signal power changes accordingly. To fully exploit the SDR dynamic range while avoiding receiver saturation, the internal transmit gain of the SDR is statically adjusted for each TX position, as indicated in Fig. 2. The gain tuning is performed considering the directive log-periodic antenna at the

RX, which provides higher antenna gain and therefore represents the worst-case condition in terms of potential receiver saturation. Once selected, the transmit gain remains fixed while sweeping over all the RIS configurations at that position and is reconfigured only when the transmitter is moved to a different location.

MEASUREMENT AND RIS SWITCHING PROCEDURE

The measurement campaign is conducted using IEEE 802.11ac VHT frames over an 80 MHz bandwidth centered at a carrier frequency of 5.530 GHz. This frequency is selected as it corresponds to the operating point at which the RIS introduces the largest phase variation [10].

While the receiver captures and stores continuously complex baseband IQ samples for offline processing in MATLAB, the transmitter operation and RIS reconfiguration follow a structured sequence of recurring phases:

- 1) *RIS Configuration and Settling*: The RIS is programmed with a given configuration pattern by setting the binary state of its unit cells. After applying the configuration, a settling time of approximately 0.3 s is enforced before transmission, ensuring the RIS enough time for changing the configuration.
- 2) *Frame Generation and Payload Tagging*: Wi-Fi frames are generated in MATLAB, each one embedding an identifier corresponding to the active RIS configuration, written at a fixed payload offset. This enables an unambiguous association between received frames and RIS states during post-processing.
- 3) *Transmission Window*: The TX streams the generated waveform continuously for approximately 0.6 s, while keeping the RIS configuration fixed. During this interval, the RX collects approximately 60 frames (thus, 60 CSI samples per receiving antenna) per RIS configuration.
- 4) *Silence Window and Repetition*: After the transmission window, the TX is configured to transmit zeros (i.e., remain effectively silent) for approximately 0.3 s. This silence interval facilitates temporal separation between consecutive RIS configurations and simplifies the segmentation and parsing of the received data during offline processing. Upon completion of this interval, the procedure resumes from Phase 1.

The above procedure is repeated for all considered RIS configurations and for nine different TX positions, while keeping the RX and RIS locations fixed, as illustrated in Fig. 2.

Exploring the Configuration Space of the RIS

Given the extremely large configuration space of the 256-element binary RIS, a structured exploration strategy is adopted to balance analytical tractability and measurement diversity within a single measurement campaign.

The first 16 configurations are obtained by partitioning the surface into four square macro-blocks of 8×8 elements. All elements within the same macro-block share the same state (ON or OFF), so that the RIS can be virtually regarded as a four-element surface. This reduced representation enables a tractable analysis of channel behavior and facilitates the

¹<https://kb.ettus.com/X300/X310>

²https://kb.ettus.com/OctoClock_CDA-2990

³<https://aaronia.com/en/log-periodic-antenna-hyperlog7060>

⁴<https://aaronia.com/en/breitbandantenne-hyperlog30100>

TABLE I
EXPERIMENTAL SETUP AND MEASUREMENT PARAMETERS

Experimental detail	Description
Carrier frequency	5.530 GHz
Signal bandwidth	80 MHz (IEEE 802.11ac VHT)
Recorded signals	Complex baseband IQ samples
Extracted metric	CSI
RIS elements	256 (16×16 array)
RIS control	1-bit per element (binary states)
RIS operating band	5.150 GHz to 5.875 GHz
RIS size	400 mm × 320 mm
Unit-cell architecture	3-layer PCB with CMOS SPDT switch
SDR platforms	2× Ettus USRP X310
SDR synchronization	External OctoClock (10 MHz + PPS)
TX antenna	Log-periodic (HyperLOG 60100)
RX antennas	Log-periodic (HyperLOG 30100) and dipole
RX SDR gain	35 dB (fixed, AGC off)
TX external amplifier	25 dB gain, 2 W max output
TX positions	9
TX SDR gain	Individually adjusted for each TX position
RIS configurations	10 000 per TX position
Frames per configuration	≈ 60
RIS settling time	0.3 s (conservative waiting time after reconfiguration)
Transmission window	0.6 s
Silence interval	0.3 s
Environment	Controlled indoor with RF absorbers

validation of simple linear models. In this setting, all possible $2^4 = 16$ combinations of the macro-block states are exhaustively explored.

Subsequently, the surface is divided into nine macro-blocks arranged in a 3×3 grid. The first two macro-rows and macro-columns consist of 5 elements each, while the third macro-row and macro-column consist of 6 elements each. Also in this case, all $2^9 = 512$ possible combinations of the macro-block states are measured. The remaining configurations are generated by independently assigning the ON/OFF state to each element. Overall, this progressive strategy, from coarse macro-block control to fully random element-wise configurations, results in 10 000 distinct RIS configurations explored for each TX position.

A summary of the main experimental parameters is reported in Table I.

DATASET ANALYSIS

We start the analysis recalling that the RIS we employed for our experiments is described in [10] and comprises unit cells with a *binary*-switchable resonance frequency, enabling two different reflection coefficients with different phases corresponding to the two switching states. The RIS introduces a change of phase and magnitude when the elements are ON and OFF, and such a change depends on the operating frequency. We now want to find the relation between the selected configuration and the effects on the cascade channel of the signal passing through the RIS.

Stimulated by the experimental results, we first observed that even in the absence of LOS between TX and RX and

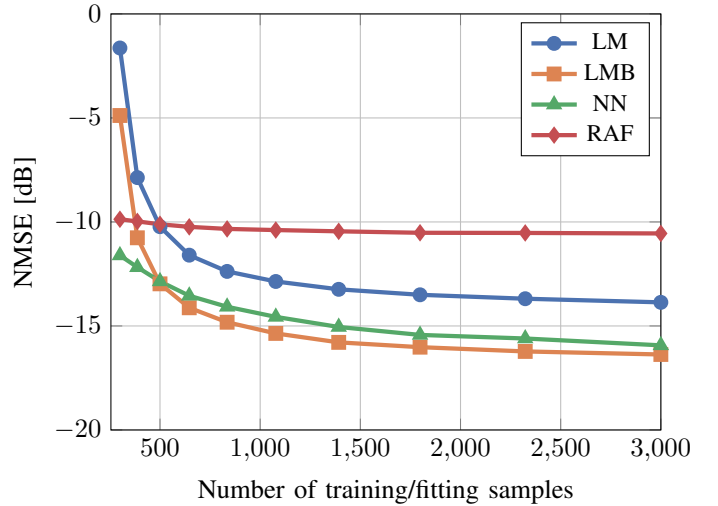


Fig. 3. NMSE for different models as a function of the number of fitting (or training) samples.

without a major reflector, a fixed component was present in the channel, which could not be controlled by changing the configuration. This effect is due to the frame of the RIS and other parts that are not controllable and can be modeled as a channel bias. Then, to model the impact of configuration on the channel, we consider two options. The first approach employs a simple linear model (LM) that maps the vector of the RIS elements' response, each modeled as a complex-valued symbol from a binary alphabet, to the resulting channel. When the bias is considered, we obtain the linear model with bias (LMB). The second is a general non-linear model (NLM), where different machine learning (ML) models, namely neural network (NN) or random forest (RAF), are used to infer the resulting channel from the chosen configuration, using part of the BRISC dataset for training.

Model Validation

To validate the models, we used multiple CSI samples along with their respective RIS configurations to fit/train the different approaches. We also considered testing channels associated with unseen configurations to assess the predictive capacity of the model. To construct such a dataset, we pre-processed the measured CSI by averaging the channels that correspond to the same configuration, to reduce the noise impact. Performance is quantified through the average L_2 error between the predicted and measured CSI, normalized by the average L_2 norm of the measured CSI. In the following, we used the CSI corresponding to the log-periodic receiving antenna, as the dipole CSI leads to the same conclusions.

Linear Models: to validate LM and LMB, we employed Ridge regression to estimate the composite channel constituted by the Khatri-Rhao product of the TX-RIS and RIS-RX channels. This composite channel can be used to obtain the TX-RIS-RX channel for any RIS configuration, [11]. This approach is more robust than the simple least squares (LS) solution thanks to the regularization term.

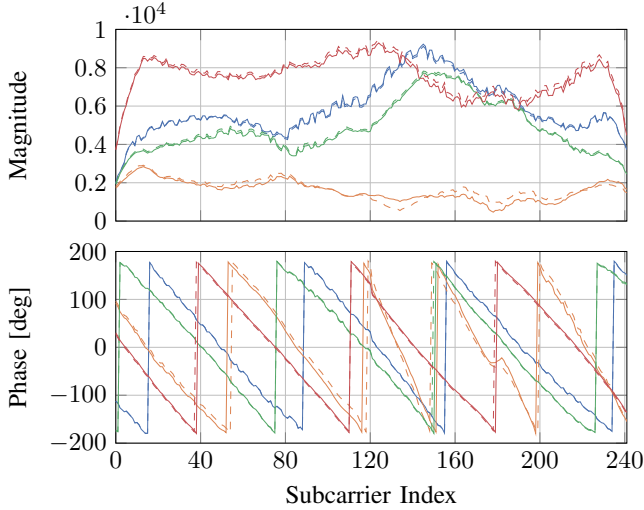


Fig. 4. Magnitude (top) and phase (bottom) for 4 different RIS configurations. The solid line represents the predicted channels, while the dashed lines refer to the measured ones.

Non-linear Models: to capture the non-linear mapping between RIS configurations and resulting CSI we employed two state-of-the-art data-driven approaches, namely NN and RAF. We chose a NN for its universal approximation capabilities and RAF as an ensemble learning strategy suitable for regression tasks when dealing with binary inputs, since each element phase profile can be encoded with 1 if it is ON, 0 otherwise.

Fig. 3 shows the reconstruction normalized mean-square-error (NMSE), normalized to the CSI power, for different sizes of the fitting/training data. The training dataset was randomly permuted, while testing was performed on the last 2000 channels. We see that all models achieve good performance in terms of error, with the NLMs outperforming the linear models when a small number of training configurations is used.

Fig. 4 shows the reconstructed CSI with LMB using the first 300 configurations to fit the model, which was then tested on the subsequent 200 configurations (from configuration 301 to 501), where no random permutation was performed. In this setting LMB achieves an NMSE of -20.57 dB, which is less than the one in Fig. 3 for the same number of fitting samples. This suggests that linear models are more effective when we randomly change blocks of elements, rather than changing single elements at random. In fact, changing blocks of elements causes a higher diversity in the resulting channels when compared to configurations where all elements change randomly, and this helps the linear models to better fit the data.

USE CASE: PHYSICAL-LAYER AUTHENTICATION

First, we note that the TX-RIS-RX channel is highly sensitive to the geometry of the environment and the relative positions of the communication devices. Even small variations in the position of the transmitter might produce measurable changes in the channel response experienced at the receiver. This feature provides a location-dependent signature that is

difficult for a malicious node to replicate and lays the foundation for PLA techniques.

In tag-based PLA schemes, authentication relies on verifying that successive transmissions originate from the same position, i.e., they exhibit similar characteristics, taking into account estimation noise and possible variations in channel conditions due to the movement of surrounding objects [12]. The reconfigurable nature of an RIS further strengthens the tag-based PLA since it can be configured to probe specific propagation paths, tagging the legitimate transmitter with a spatial signature that enhances separability from adversaries [13].

Moreover, RISs enable a new challenge-response (CR)-PLA mechanism, where the verifier randomly selects an RIS configuration that acts as an authentication challenge. The resulting channel response serves as proof of legitimacy, since only a legitimate transmitter can reproduce the corresponding channel characteristics [14], [15]. In both tag- and CR-based PLA, the RIS increases the unpredictability and spatial selectivity of the authentication process, significantly increasing the difficulty for an adversary attempting impersonation.

We now discuss a representative use case of the proposed BRISC dataset in the context of PLA. We consider a legitimate device (Alice) transmitting to a legitimate receiver (Bob), while a third device (Eve) aims at sending messages to Bob by impersonating Alice. PLA is the security mechanism by which Bob decides if the messages received are coming from Alice or not. We consider Alice and Bob as static devices and let Bob use CSI to make the decision. In this process, we also exploit the possibility of reconfiguring the RIS to make authentication more accurate. The PLA mechanisms work as follows. In a preliminary phase, Alice transmits some known pilot signal to Bob, who takes advantage of its knowledge to obtain a noisy estimate of the Alice-Bob channel. We assume that such a phase is authenticated at a higher layer (thus, it provides a reliable channel estimate) and has to be repeated every time the Alice-Bob channel changes significantly. In the subsequent phase, upon reception of a signal, Bob estimates the channel over which such a signal traveled, obtaining the estimate of the Alice-Bob channel. Then, Bob performs a test on the obtained estimate to decide whether the transmitter was Alice or not.

Our goal is to show how the measured RIS-assisted CSI can be exploited to distinguish between a legitimate transmitter Alice and an impersonating device Eve. In the indoor scenario considered, Alice occupies one of the 9 positions, while the remaining positions represent potential adversarial locations. The CSI samples collected at each position capture the joint effects of indoor multipath propagation, spatial geometry, and RIS configuration. As a result, transmissions originating from different positions produce distinguishable channel signatures, which can be exploited for authentication. This setup allows a systematic evaluation of authentication performance across an Alice-Eve position pair, providing a realistic representation of spatial impersonation attempts in RIS-assisted indoor environments.

In the proposed PLA framework, we first identify a subset of RIS configurations and subsequently assess the security

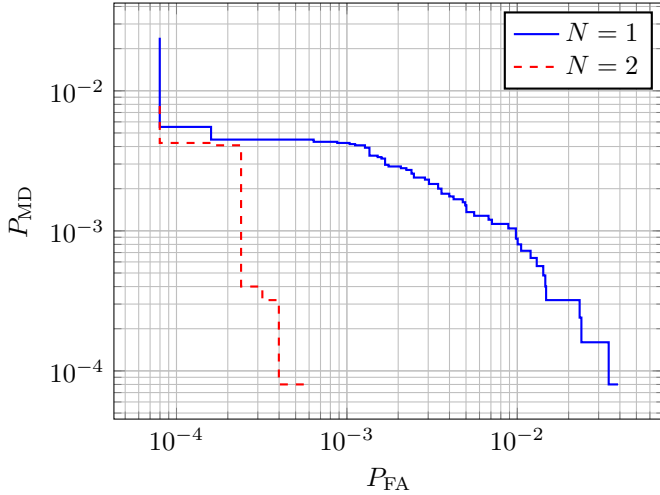


Fig. 5. Empirical DET curves obtained by selecting RIS configurations based on a capacity threshold and by varying the number of channel subcarriers used for authentication N . Only those configurations that limit the rate reduction to a maximum of 10% have been used. Alice and Eve have been considered in positions 1 and 4, respectively.

performance for these selections. To optimize the configuration selection process, we identify the specific RIS profile that maximizes the achievable communication rate. We then retain only those configurations that limit the rate reduction to a maximum of 10%. This constraint ensures that the authentication procedure utilizes RIS configurations that maintain high communication performance, preventing authentication enhancements from compromising the underlying transmission quality.

Performance is evaluated using detection error tradeoff (DET) curves, which provide a complete view of the authentication capability achieved. Specifically, the DET curve reports the tradeoff between the probability that receiver Bob tags a legitimate message from Alice as malicious (probability of false alarm P_{FA}) and the probability that the receiver Bob accepts a message from Eve as legitimate (probability of missed detection P_{MD}) obtained by varying the decision threshold of the authentication test.

Moreover, we investigate how the dimensionality of the CSI representation affects the authentication performance by limiting the number of subcarriers used in the detector. This dimensionality reduction aims at assessing how much spectral information is required to reliably separate Alice and Eve.

Fig. 5 shows the DET curves obtained by selecting RIS configurations based on a capacity threshold and varying the number of channel subcarriers N used for authentication. Specifically, only configurations achieving at least 90% of the maximum capacity are retained. It can be seen that even a minimal number of subcarriers is sufficient to achieve strong discrimination, and increasing the dimensionality from 1 to 2 subcarriers produces a significant improvement in the authentication performance. Beyond this point, performance saturates, indicating that most of the discriminative information is already captured.

CONCLUSIONS

This article introduced BRISC, a comprehensive measurement-based dataset for RIS-assisted 80 MHz wireless channels in an indoor environment at 5.530 GHz. By systematically exploring thousands of RIS configurations across multiple transmitter locations, BRISC captures the joint impact of RIS control, multipath propagation, and spatial geometry under realistic conditions. The dataset was shown to be effective both for calibrating and validating state-of-the-art RIS channel models, highlighting the trade-offs between linear and data-driven approaches in terms of accuracy and training requirements. Specifically, a linear model with incorporated bias has been shown to perform similarly, if not even better than a neural network for the channel frequency response reconstruction task. Furthermore, a representative physical-layer authentication use case demonstrated that RIS-assisted channels provide strong spatial discrimination, even when relying on a limited number of subcarriers. Overall, BRISC constitutes a valuable experimental benchmark for the design, validation, and comparison of signal processing, learning, and security techniques for RIS-enabled wireless systems.

ACKNOWLEDGMENT

We thank Prof. Aydin Sezgin of the Ruhr-Bochum University (Germany) for having provided the RIS used for the experiments.

REFERENCES

- [1] J. Xiao, "RIS_CE," IEEE Dataport, 2023. [Online]. Available: <https://dx.doi.org/10.21227/3c2t-dz81>
- [2] M. Piana, G. Alghisi, A. Guglielmi, G. Perin, F. Gringoli, and S. Tomasin, "BRISC_RIS_dataset_scripts," GitHub, 2026. [Online]. Available: https://github.com/MattiaP1999/BRISC_RIS_dataset_scripts
- [3] —, "BRISC: A dataset of channel measurements with a reflective intelligent surface at 5 GHz," Zenodo, 2026. [Online]. Available: <https://zenodo.org/records/18714621>
- [4] Y. Liu, X. Liu, X. Mu, T. Hou, J. Xu, M. Di Renzo, and N. Al-Dhahir, "Reconfigurable intelligent surfaces: Principles and opportunities," *IEEE Commun. Surveys Tuts.*, vol. 23, no. 3, pp. 1546–1577, 2021.
- [5] Q. Wu and R. Zhang, "Intelligent reflecting surface enhanced wireless network: Joint active and passive beamforming design," in *Proc. of 2018 IEEE Global Commun. Conf. (GLOBECOM)*, 2018, pp. 1–6.
- [6] A. Almohamad, A. M. Tahir, A. Al-Kababji, H. M. Furqan, T. Khatlab, M. O. Hasna, and H. Arslan, "Smart and secure wireless communications via reflecting intelligent surfaces: A short survey," *IEEE Open J. Commun. Soc.*, vol. 1, pp. 1442–1456, Sep. 2020.
- [7] H. Niu, Z. Chu, F. Zhou, and Z. Zhu, "Simultaneous transmission and reflection reconfigurable intelligent surface assisted secrecy MISO networks," *IEEE Commun. Lett.*, vol. 25, no. 11, pp. 3498–3502, Nov. 2021.
- [8] H. Niu, Z. Lin, Z. Chu, Z. Zhu, P. Xiao, H. X. Nguyen, I. Lee, and N. Al-Dhahir, "Joint beamforming design for secure RIS-assisted IoT networks," *IEEE Internet Things J.*, vol. 10, no. 2, pp. 1628–1641, Feb. 2023.
- [9] S. Tewes, M. Heinrichs, K. Weinberger, R. Kronberger, and A. Sezgin, "A comprehensive dataset of RIS-based channel measurements in the 5 GHz band," in *Proc. of 2023 IEEE Veh. Technol. Conf. (VTC2023-Spring)*, 2023, pp. 1–5.
- [10] M. Heinrichs, A. Sezgin, and R. Kronberger, "Open source reconfigurable intelligent surface for the frequency range of 5 GHz WiFi," in *Proc. of 2023 IEEE Int. Symp. Ant. Propag. (ISAP)*, 2023, pp. 1–2.
- [11] K. F. Masood, J. Tong, J. Xi, J. Yuan, and Y. Yu, "Inductive matrix completion and root-MUSIC-based channel estimation for intelligent reflecting surface (RIS)-aided hybrid MIMO systems," *IEEE Trans. Wireless Commun.*, vol. 22, no. 11, pp. 7917–7931, Mar. 2023.

- [12] J. Zhang, F. Ardizzon, M. Piana, G. Shen, and S. Tomasin, "Physical layer-based device fingerprinting for wireless security: From theory to practice," *IEEE Trans. Inf. Forensics Security*, vol. 20, pp. 5296–5325, 2025.
- [13] P. Zhang, Y. Teng, Y. Shen, X. Jiang, and F. Xiao, "Tag-based PHY-layer authentication for RIS-assisted communication systems," *IEEE Trans. on Dependable and Secure Comput.*, pp. 1–15, Jan. 2023.
- [14] A. V. Guglielmi, L. Crosara, S. Tomasin, and N. Laurenti, "Physical-layer challenge-response authentication with IRS and single-antenna devices," in *Proc. of 2024 IEEE Int. Conf. Commun. Worksh. (ICC worksh.)*, 2024.
- [15] S. Tomasin, T. N. M. M. Elwakeel, A. V. Guglielmi, R. Maes, N. Noels, and M. Moeneclaey, "Analysis of challenge-response authentication with reconfigurable intelligent surfaces," *IEEE Trans. Inf. Forensics Security*, vol. 19, pp. 9494–9507, Sep. 2024.

BIOGRAPHIES

Mattia Piana (mattia.piana@phd.unipd.it, Graduate Student Member, IEEE) is currently a Ph.D. student at the University of Padova, and his research interests include physical layer security and reflective intelligent surfaces

Giovanni Angelo Alghisi (giovanni.alghisi@unibs.it, IEEE Student Member) is a Ph.D. student at the University of Brescia. His research interests include physical-layer security and privacy in Wi-Fi networks, CSI-based sensing, and Wi-Fi-based indoor localization.

Anna Valeria Guglielmi (annavaleria.guglielmi@unipd.it) is an assistant professor at the University of Padova, Italy. Her current research interests include machine-learning architectures and signal processing for wireless communication systems and physical layer security.

Giovanni Perin (giovanni.perin@unibs.it, IEEE Member) is an assistant professor at the University of Brescia, Italy. His current research focuses on distributed learning and optimization, wireless network sustainability, and wireless sensing and security.

Francesco Gringoli (francesco.gringoli@unibs.it, IEEE Senior Member) is a full professor at the University of Brescia, Italy. His research interests include security assessment, performance evaluation, and medium access control in Wireless LANs.

Stefano Tomasin (stefano.tomasin@unipd.it) is a full professor at the University of Padova, Italy. His interests include signal processing for communications and physical layer security. From 2020 to 2023, he was an Editor of the IEEE Transactions on Information Forensics and Security, and from 2023, he is deputy editor in chief of the same journal.